AIP Applied Physics Letters

Phonon and electron transport through Ge2Sb2Te5 films and interfaces bounded by metals

Jaeho Lee, Elah Bozorg-Grayeli, SangBum Kim, Mehdi Asheghi, H.-S. Philip Wong et al.

Citation: Appl. Phys. Lett. **102**, 191911 (2013); doi: 10.1063/1.4807141
View online: http://dx.doi.org/10.1063/1.4807141
View Table of Contents: http://apl.aip.org/resource/1/APPLAB/v102/i19
Published by the American Institute of Physics.

Additional information on Appl. Phys. Lett.

Journal Homepage: http://apl.aip.org/
Journal Information: http://apl.aip.org/about/about_the_journal
Top downloads: http://apl.aip.org/features/most_downloaded
Information for Authors: http://apl.aip.org/authors

ADVERTISEMENT

APPLIED PHYSICS LETTERS 102, 191911 (2013)

Phonon and electron transport through $Ge_2Sb_2Te_5$ films and interfaces bounded by metals

Jaeho Lee,[1] Elah Bozorg-Grayeli,[1] SangBum Kim,[2] Mehdi Asheghi,[1] H.-S. Philip Wong,[3] and Kenneth E. Goodson[1]

[1]Department of Mechanical Engineering, Stanford University, Stanford, California 94305, USA
[2]IBM T. J. Watson Research Center, Yorktown Heights, New York 10598, USA
[3]Department of Electrical Engineering, Stanford University, Stanford, California 94305, USA

(Received 4 March 2013; accepted 3 May 2013; published online 16 May 2013)

While atomic vibrations dominate thermal conduction in the amorphous and face-centered cubic phases of $Ge_2Sb_2Te_5$, electrons dominate in the hexagonal closed-packed (hcp) phase. Here we separate the electron and phonon contributions to the interface and volume thermal resistances for the three phases using time-domain thermoreflectance and electrical contact resistance measurements. Even when electrons dominate film-normal volume conduction (i.e., 70% for the hcp phase), their contribution to interface heat conduction is overwhelmed by phonons for high-quality interfaces with metallic TiN. © *2013 AIP Publishing LLC*. [http://dx.doi.org/10.1063/1.4807141]

Chalcogenide phase change materials, known primarily through their application in optical data storage, are receiving renewed interest for applications in electronic memory due to their unusual electrical properties. The amorphous phase can be transformed into one or more crystalline phases through electrical heating. The rapid and repeatable switching among phases provides a remarkable contrast in the electrical resistivity and modifies the contribution of electrons to thermal conduction. The chalcogenide compound $Ge_2Sb_2Te_5$ provides a special opportunity to study parallel heat conduction by electrons and phonons. Two crystalline phases feature similar acoustic properties but dramatically different electrical conductivities and, in the hexagonal close packed phase, electrons and phonons contribute comparably to heat conduction. When bounded by metals in thin film form, $Ge_2Sb_2Te_5$ provides the further opportunity to examine near-interfacial electron-phonon coupling and energy conversion through the electrical and thermal boundary resistances. There are thermal conductivity data for films of $Ge_2Sb_2Te_5$ in its various phases[1–15] and even dedicated studies of the interface resistance of these films with dielectrics[2,7,11,15] and metals.[13] However, a study of the complex interplay of electron and phonon transport within the volume and through the interface requires parallel electrical transport measurements of the volume and interface in these films. Here, we use electrical and thermal measurements to separate the electron and phonon contributions to thermal transport of $Ge_2Sb_2Te_5$ films in the amorphous, face-centered cubic (fcc), and hexagonal close-packed (hcp) phases. We select TiN as the bounding metal conductor owing to the extensive additional characterization of this specific electrical conductor for phase change memory application.[16] For clarity here, we refer to phonon transport in all three phases even though this approach is questionable for the amorphous phase considering the short mean free path values compared to the wavelength.

The thermal conductivity and thermal boundary resistance are measured by picosecond time-domain thermoreflectance, which captures the unique signatures in the temporal temperature decay associated with the film and the interface, respectively. The electrical resistivity and specific contact resistance are each measured by three independent techniques including the Cross-Bridge Kelvin Resistor (CBKR), and Linear and Circular Transfer Length Methods.

Samples for the heat conduction measurements are prepared by depositing blanket films of TiN, $Ge_2Sb_2Te_5$, and TiN without breaking the vacuum (Fig. 1). The $Ge_2Sb_2Te_5$ films are deposited by sputtering in argon ambient at chamber pressure 5 mT for the thicknesses of 30 nm and 150 nm. A 50-nm aluminum (Al) film is deposited as a photothermal transducer layer. Samples for the electrical measurements are prepared by patterning $Ge_2Sb_2Te_5$ and TiN electrodes designed for each measurement technique (Fig. 2). The samples are deposited at room temperature and annealed at varying temperatures from 25 °C to 300 °C before the measurements.

Picosecond time-domain thermoreflectance temporally confines the heated region to the TiN-$Ge_2Sb_2Te_5$-TiN sandwich structure (Fig. 1). The thermoreflectance experimental details for can be found elsewhere.[17] The thermal properties at different points within the stack affect different time domains of the thermal decay trace. From ~0.5 to ~2.5 ns after the pump pulse arrives, the thermal resistance of the top TiN layer and underlying $Ge_2Sb_2Te_5$ dictate the decay

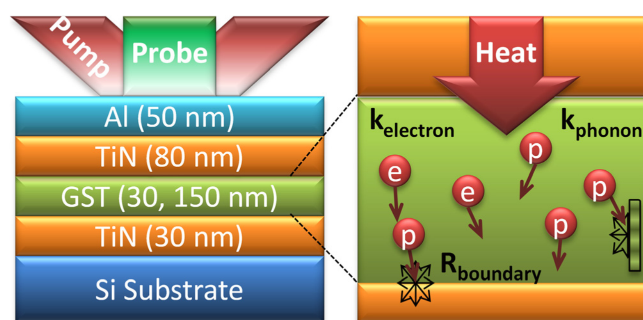

FIG. 1. Pump-and-probe thermoreflectance measurement sample geometry (left) and the thermal conduction model (right) for $Ge_2Sb_2Te_5$ (GST) films. The electrons (e) and phonons (p) carry the heat across the film and the interfaces while interacting with each other and with microstructural defects and phase impurities.

 © 2013 AIP Publishing LLC

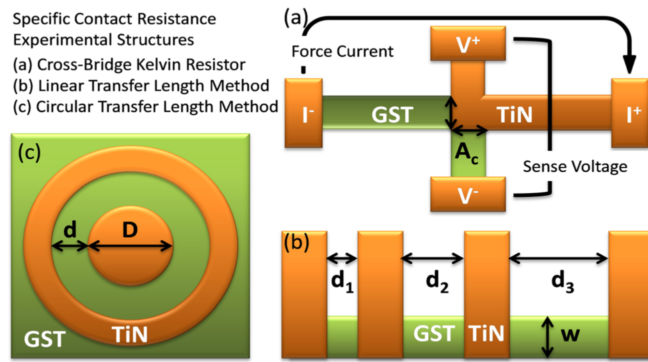

FIG. 2. (a) The Cross-Bridge Kelvin Resistor method allows direct access to the interfacial voltage and the current across an overlapping area of 10-μm by 10-μm. (b) The Linear Transfer Length Method extracts the contact resistance from a 100-μm-wide $Ge_2Sb_2Te_5$ leg with intermittent TiN contacts with a gap spacing (6 μm ~ 60 μm). (c) The Circular Transfer Length Method extracts the contact resistance from an inner circular TiN of diameter 100 μm on a $Ge_2Sb_2Te_5$ film with a ring-shaped spacing (2 μ ~ 23 μm).

behavior. Using the measured thermal conductivity of TiN, we extract a combination of the intrinsic $Ge_2Sb_2Te_5$ thermal resistance and the top $Ge_2Sb_2Te_5$-TiN thermal boundary resistance. The thermal decay behavior from ~2.5 ns to before the arrival of the next pump pulse is sensitive to the total resistance of the TiN-$Ge_2Sb_2Te_5$-TiN stack. Assuming the thermal boundary resistances at both $Ge_2Sb_2Te_5$-TiN interfaces are identical, we can separate out the intrinsic $Ge_2Sb_2Te_5$ thermal conductivity. The transmission electron microcopy[14] validated that roughness and phase distribution near top and bottom interfaces are nearly identical for $Ge_2Sb_2Te_5$ films that are deposited as amorphous phase and interfaced with same materials at the top and the bottom.

The interfacial form of the Wiedemann-Franz Law (WFL) has been verified recently through experiments on bimetal interfaces.[18] Here we extract the electron component from a bilayer in which phonon transport is likely significant. We measure the electrical contact properties using three techniques that are standard in the electrical engineering community. The Cross-Bridge Kelvin Resistor structure (Fig. 2(a)) allows direct measurement of specific contact resistance by forcing the current through one pair of $Ge_2Sb_2Te_5$ and TiN legs and measuring the contact voltage in the other pair of legs.[19,20] The contact area misalignment due to process variations and lateral current crowding effect can lead to measurement errors.[20,21] The linear transfer length method (TLM) structure (Fig. 2(b)) measures both the electrical resistivity and the specific contact resistance (ρ_c) by utilizing the transfer length (l_t), which is defined as the distance the current flows through $Ge_2Sb_2Te_5$ under the TiN contact. Assuming the sheet resistance (R_{sh}) of $Ge_2Sb_2Te_5$ is much larger than that of TiN, the transfer length can be estimated by $l_t = (\rho_c/R_{sh})^{1/2}$. The specific contact resistance is extracted from the measured resistances as a function of the gap spacing, assuming all contacts are identical. Since the linear-TLM structures can be affected by parasitic current in non-isolated regions, we also used the circular-TLM (Fig. 2(c)). Compared to the CBKR, the TLMs are more suitable for non-uniform contact resistances and less sensitive to the misalignment, but the uncertainty depends on the sheet resistance measurement. The three independent measurement techniques validate the results for each other and offer consistent information.

X-ray diffraction (XRD) provides information about the crystal structure for $Ge_2Sb_2Te_5$ films at different temperatures (Fig. 3). The $Ge_2Sb_2Te_5$ films deposited at room temperature are amorphous and show no observable crystal peaks up 100 °C. The $Ge_2Sb_2Te_5$ films begin crystallize to the fcc phase at temperatures from 110 to 150 °C depending on the annealing time and the film thickness. Figure 3 compares the XRD data for $Ge_2Sb_2Te_5$ films of two different thicknesses at some representative temperatures and clearly shows that the 30-nm-thick $Ge_2Sb_2Te_5$ film has higher phase transition temperatures compared to the 150-nm-thick $Ge_2Sb_2Te_5$ film. The XRD data with a full range of temperatures in an increment of 10 °C can be found in Ref. 39. The suppressed crystallization in the thinner film is believed to be due to the compressive stresses exerted by the bounding TiN films, and similar behaviors have been observed for $Ge_2Sb_2Te_5$ films with thickness below 50 nm.[22–25] The phase transition temperatures of $Ge_2Sb_2Te_5$ films interfaced with TiN[24] or Al_2O_3[25] increase with decreasing film thickness. In contrast, the phase-transition temperatures of $Ge_2Sb_2Te_5$ films interfaced with SiO_2[22,23] or ZnS-SiO_2[24] decrease with decreasing film thickness. The thickness dependent crystallization can have a very large impact on the $Ge_2Sb_2Te_5$ films in particular to their electron transport properties of such as the electrical resistivity and the Seebeck coefficient.[23]

Figure 4 shows the phase dependent thermal conductivity and the thermal boundary resistance of $Ge_2Sb_2Te_5$ films measured at room temperature after annealing at varying temperatures. The pre-annealing time is set to 10 min, and this allows crystallization to the fcc phase in both 30-nm and 150-nm-thick $Ge_2Sb_2Te_5$ films at 130 °C and transforms the 150-nm-thick $Ge_2Sb_2Te_5$ film to the hcp films at temperatures greater than 190 °C. Upon the phase transition from amorphous to fcc, the thermal conductivity of $Ge_2Sb_2Te_5$ films increases from 0.25 $W m^{-1} K^{-1}$ to 0.42 $W m^{-1} K^{-1}$. Similar increase in the thermal conductivity has been

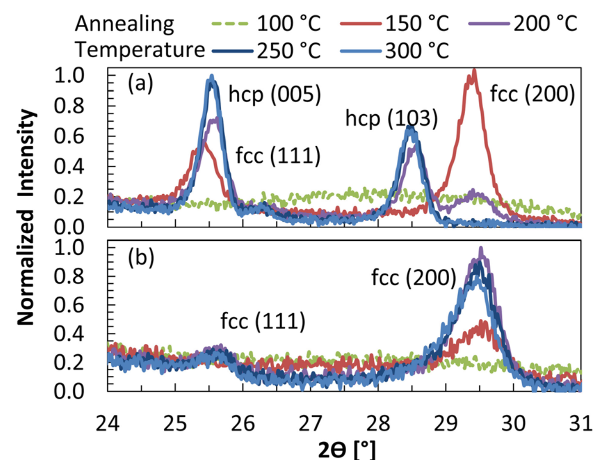

FIG. 3. Impact of annealing on the phase distributions for the (a) 150-nm-thick $Ge_2Sb_2Te_5$ film and the (b) 30-nm-thick $Ge_2Sb_2Te_5$ film, observed using X-ray diffraction with using Cu Ka radiation with a temperature increment of 10 °C in 5 min. The peaks are normalized with respect to the highest peak in each sample. The suppressed crystallization in the thinner film is due to the increased role of TiN interfaces exerting compressive stresses on $Ge_2Sb_2Te_5$.

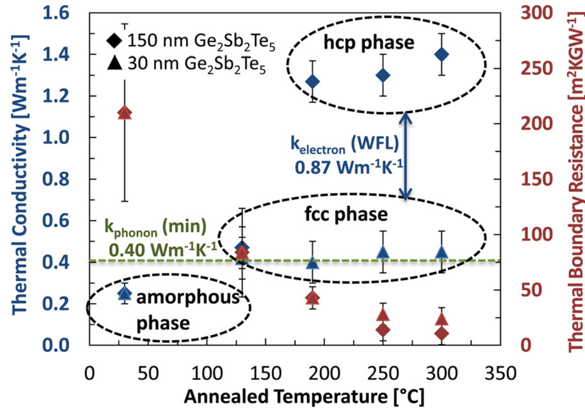

FIG. 4. Room temperature thermal conductivity and thermal boundary resistance of $Ge_2Sb_2Te_5$ films as functions of annealing temperature. While the thermal conductivity of fcc phase agrees well with the minimum thermal conductivity law, the thermal conductivity of hcp phase is much larger due to electron transport predicted by the WFL. However, the thermal boundary resistances of the both phases are similar because phonons govern thermal transport across the interfaces.

reported in many studies[1–15] including our prior work[6,13–15] and attributed to enhanced acoustic properties of the fcc phase. The data for amorphous and highly disordered crystalline materials agree well with predictions from the minimum thermal conductivity model, which describes thermal transport as a random walk of localized oscillators.[26] At temperatures greater than the Debye temperature, a model for the minimum thermal conductivity can be expressed as

$$k_{\min} = \frac{1}{2}\left(\frac{\pi}{6}\right)^{1/3} k_B {n_a}^{2/3}(v_l + 2v_t), \tag{1}$$

where k_B is the Boltzmann number, n_a is the atomic density, v_l and v_t are the longitudinal and transverse sound velocities, respectively. Using independent reports of the acoustic properties of $Ge_2Sb_2Te_5$ such as mass density and elastic modulus,[4,36] the Debye temperature $(T_D = \hbar v_s(6\pi n_a)^{1/3}/k_B)$ is estimated to be 150 K in the amorphous phase, 220 K in the fcc phase, and 230 K in the hcp phase. This indicates the available vibrational states are essentially occupied at room temperature and is consistent with our heat capacity measurements.[14] The minimum thermal conductivity for $Ge_2Sb_2Te_5$ films is estimated to be 0.27 $Wm^{-1}K^{-1}$ in the amorphous phase, 0.40 $Wm^{-1}K^{-1}$ in the fcc phase, and 0.42 $Wm^{-1}K^{-1}$ in the hcp phase. The close match of Eq. (1) with our data in the amorphous and fcc phases suggests that atomic vibrations govern transport. The acoustic properties of the hcp and fcc phases are very similar. The hcp phase, however, has a thermal conductivity well above the value determined using Eq. (1), and this is additional contribution is almost certainly due to the dramatic difference in the electron transport properties of the two phases.

The WFL has been used to estimate electron contribution to the thermal conductivities of metals, semi-metals, metallic alloys, and degenerate semiconductors including chalcogenide materials.[8,18,27–29] The WFL has recently been extended to metal films of thickness down to 7 nm[29] and to metal-metal interfaces.[18] The literature, on balance, does support the application of the WFL with the Sommerfeld value of the Lorenz number ($L_o = 2.44 \times 10^{-8}$ $W\Omega K^{-2}$)

TABLE I. Thermal conductivity of $Ge_2Sb_2Te_5$ films.

$Ge_2Sb_2Te_5$ phase	k (data) [$W\,m^{-1}\,K^{-1}$]	k_e (WFL) [$W\,m^{-1}\,K^{-1}$]	k_p (Eq. (1)) [$W\,m^{-1}\,K^{-1}$]
Amorphous	0.25 ± 0.05	0.00	0.27
Cubic (fcc)	0.45 ± 0.09	0.04	0.40
Hexagonal (hcp)	1.32 ± 0.18	0.87	0.42

for the case of degenerate semiconductors when the carrier concentration is higher than $10^{19}\,cm^{-3}$ at room temperature.[28] The carrier concentration of our hcp $Ge_2Sb_2Te_5$ films ranges from $8.2 \times 10^{19}\,cm^{-3}$ to $1.5 \times 10^{20}\,cm^{-3}$.[23] The WFL ($k_e = (L_oT)/\rho$) and the electrical resistivity (ρ) data show that the electron contribution to the thermal conductivity in $Ge_2Sb_2Te_5$ films is negligible in the amorphous phase but increases up to 13% in the fcc phase and up to 70% in the hcp phase. For hcp $Ge_2Sb_2Te_5$ films, the presence of a significant electron contribution to the thermal conductivity, 0.87 $Wm^{-1}K^{-1}$ estimated by the WFL and our measured electrical resistivity ($8.39 \times 10^{-6}\,\Omega$-m), explains the large increase in the measured thermal conductivity. The thermal conductivity in the hcp phase increases with increasing annealing temperature due to the increase in the carrier concentration and to the reduction in the concentration of other phases. This is consistent with our electrical resistivity data and previous work on the thermoelectric properties, which demonstrated the impact of carrier concentration and phase purity on electron transport.[23] Table I summarizes the thermal conductivity findings and shows the significantly increased role of electron transport in the hcp phase. We find much support for this hypothesis from complementary predictions of the phonon thermal conductivity (Eq. (1)) and the electron thermal conductivity (WFL), as described above. While previous studies make similar assessment for the crystalline phases,[3,4,8] this is the only report considering the intrinsic components of thermal and electrical transport by separating out the respective interface contributions.

The thermal boundary resistance of the fcc and the hcp $Ge_2Sb_2Te_5$ films cannot be distinguished considering the experimental uncertainty (Fig. 4). This is not surprising considering the similar acoustic properties in the two phases, but raises questions about the importance of the electron transport through the interface. The electron thermal boundary resistance ($R_{b,e}$) can be estimated by the boundary form of Wiedemann-Franz Law, $R_{b,e} = \rho_c/(L_oT)$.[18,30] The electron transport across the interface of $Ge_2Sb_2Te_5$ films increases by more than five orders of magnitude after crystallization and slightly improves with higher annealing temperatures.[31] The specific contact resistance measured by the CBKR and TLM structures (see Fig. 2) for fcc $Ge_2Sb_2Te_5$ prepared by annealing at 200 °C is 84 ± 8 Ω-μm^2 and for hcp $Ge_2Sb_2Te_5$ prepared by annealing at 300 °C is 7 ± 2 Ω-μm^2. Even with the substantial reduction in the specific contact resistance, the electron transport contributes less than 2% for the boundary thermal transport. This explains the similar thermal boundary resistance in the fcc and the hcp phases despite the large contrast in thermal conductivity.

The specific contact resistance measurements for crystalline $Ge_2Sb_2Te_5$, from 25 to 300 °C, show weak dependence on the temperature and indicate that the electron transport is dominated by tunneling. Combining the electron tunneling model[32] with the WFL, we can express the electron boundary resistance as

$$R_{b,e} = \rho_{b,\infty}\exp\left(\frac{2\phi_b}{\hbar}\sqrt{\frac{m^*\varepsilon_r}{N}}\right)(L_oT)^{-1}, \quad (2)$$

where $\hbar$ is the reduced Planck's constant, ϕ_b is the barrier height, m^* is the effective mass of tunneling electrons, ε_r is the dielectric constant, N is the carrier concentration, and $\rho_{c,\infty}$ is the specific contact resistance with infinitely large carrier concentration, which is used here to simplify the form.[33] The equation shows that electron transport strongly depends on the carrier concentration (log $R_{b,e} \sim N^{-1/2}$) and the barrier height (log $R_{b,e} \sim \phi_b$). The barrier height for crystalline $Ge_2Sb_2Te_5$ does not depend on the metal work function,[31] possibly due to Fermi level pinning and the potential presence of a large trap density. Therefore, our data may suggest that the electron contribution to boundary thermal transport may generally be negligible between $Ge_2Sb_2Te_5$ and all of the likely metals with which it might be combined.

Since phonons dominate the boundary thermal transport, the diffuse mismatch (DMM) models can describe the thermal boundary resistance in different phases of $Ge_2Sb_2Te_5$ films. The DMM is a simplified approach that assumes all phonons are diffusely scattered at the interface.[37] While many variations of these models exist, the DMM using measured heat capacity data better captures experimental results for $Ge_2Sb_2Te_5$ films[13]

$$R_{b,p} = \left(\frac{\sum_j v_{2,j}^{-2}}{12\left(\sum_j v_{1,j}^{-2} + \sum_j v_{2,j}^{-2}\right)}\sum_j v_{1,j}\right)^{-1}(C_1)^{-1}, \quad (3)$$

where $R_{b,p}$ is the phonon boundary resistance, C_1 is the heat capacity of material 1, and $v_{i,j}$ is the velocity of phonon mode j in material i. The model implicitly assumes the same form of density of states on both sides of the interface and the results depend on the material assignment.[38] Since we know the heat capacity of $Ge_2Sb_2Te_5$,[14] we have assigned $Ge_2Sb_2Te_5$ to be the material 1 and TiN to be the material 2. The equation provides theoretical thermal boundary resistance values: 43 m^2K-GW^{-1} for the amorphous $Ge_2Sb_2Te_5$, 15 m^2K-GW^{-1} for the fcc $Ge_2Sb_2Te_5$, and 13 m^2K-GW^{-1} for the hcp $Ge_2Sb_2Te_5$. The DMM captures the phase dependence, which is governed by the changes in sound velocity but does not accurately match the data (Table II). The discrepancy is partly due to the fact that the original model was developed in the low temperature limit and required high quality interfaces.[37] The close match between the data and the DMM value for samples with a high temperature anneal suggests that the large mismatch for samples with a low temperature anneal is potentially due to imperfections near the interface and contacts. The process dependent defects can be reduced by high temperature deposition and their impact on thermal transport needs further investigation.

TABLE II. Thermal boundary resistance of $Ge_2Sb_2Te_5$ films.

$Ge_2Sb_2Te_5$ phase	R_b (data) [m^2 K-GW^{-1}]	$R_{b,e}$ (WFL) [m^2 K-GW^{-1}]	$R_{b,p}$ (DMM) [m^2 K-GW^{-1}]
Amorphous	210 ± 80	10^9	43
Cubic (fcc)	24 ± 10	10^4	15
Hexagonal (hcp)	12 ± 10	10^3	13

At metal-semiconductor and metal-dielectric interfaces, an additional thermal resistance may become important due to electron-phonon coupling.[34,35] We assume that direct coupling of electrons in the metal and phonons in the nonmetal at the interface does not offer a significant pathway because the electron heat capacity is about three orders of magnitude smaller than the phonon heat capacity. Since the electron boundary resistance is much greater than the phonon boundary resistance, electrons transfer energy to phonons before the phonons transfer the energy across the interface. The electron-phonon coupling can increase the overall resistance of electron dominated materials, but our data suggest that the coupling resistance is very small in $Ge_2Sb_2Te_5$ films by showing the similar thermal boundary resistance between the fcc and the hcp phases. However, at temperatures higher than the Debye temperature, i.e., 580 K for TiN,[35] the electron-phonon coupling resistance may become important because it scales by $T^{1/2}$ while phonon and electron boundary resistances do not increase with temperature.

We have separated the phonon and electron contributions to volume and interface heat conduction in the three phases of $Ge_2Sb_2Te_5$ films. While atomic vibrations dominate thermal conduction in the amorphous and the fcc films, electrons dominate in the hcp film. The phonons govern boundary thermal transport of $Ge_2Sb_2Te_5$ interfaces with TiN in all three phases including the electron dominated hcp phase. This study provides guidelines for understanding the complex interplay of electron and phonon transport for chalcogenides with metallic interfaces.

The authors J.L., E.B.-G., M.A., H.-S.P.W., and K.E.G. appreciate support from by the Air Force Office of Scientific Research through FA9550-12-1-0195, National Science Foundation through Grant No. CBET-0853350, and Intel Corporation.

[1]C. Peng, L. Cheng, and M. Mansuripur, J. Appl. Phys. **82**, 4183 (1997).
[2]E. K. Kim, S. I. Kwun, S. M. Lee, H. Seo, and J. G. Yoon, Appl. Phys. Lett. **76**, 3864 (2000).
[3]V. Giraud, J. Cluzel, V. Sousa, A. Jacquot, A. Dauscher, B. Lenoir, H. Scherrer, and S. Romer, J. Appl. Phys. **98**, 013520 (2005).
[4]H.-K. Lyeo, D. G. Cahill, B.-S. Lee, J. R. Abelson, M.-H. Kwon, K.-B. Kim, S. G. Bishop, and B.-K. Cheong, Appl. Phys. Lett. **89**, 151904 (2006).
[5]M. Kuwahara, O. Suzuki, Y. Yamakawa, N. Taketoshi, T. Yagi, P. Fons, T. Fukaya, J. Tominaga, and T. Baba, Microelectron. Eng. **84**, 1792 (2007).
[6]J. P. Reifenberg, M. A. Panzer, S.-B. Kim, A. M. Gibby, Y. Zhang, S. Wong, H.-S. P. Wong, E. Pop, and K. E. Goodson, Appl. Phys. Lett. **91**, 111904 (2007).
[7]W. P. Risk, C. T. Rettner, and S. Raoux, Rev. Sci. Instrum. **79**, 026108, (2008).
[8]W. P. Risk, C. T. Rettner, and S. Raoux, Appl. Phys. Lett. **94**, 101906 (2009).

[9]R. Fallica, J. Battaglia, S. Cocco, C. Monguzzi, A. Teren, C. Wiemer, E. Varesi, R. Cecchini, A. Gotti, and M. Fanciulli, J. Chem. Eng. Data **54**, 1698 (2009).
[10]T. Y. Lee, K. H. P. Kim, D.-S. Suh, C. Kim, Y.-S. Kang, D. G. Cahill, D. Lee, M.-H. Lee, M.-H. Kwon, K.-B. Kim, and Y. Khang, Appl. Phys. Lett. **94**(24), 243103 (2009).
[11]J.-L. Battaglia, A. Kusiak, V. Schick, A. Cappella, C. Wiemer, M. Longo, and E. Varesi, J. Appl. Phys. **107**, 044314 (2010).
[12]D. Lee, S. S. Yim, H. K. Lyeo, M. H. Kwon, D. Kang, H. G. Jun, S. W. Nam, and K. B. Kim, Electrochem. Solid-State Lett. **13**(2), K8 (2010).
[13]J. P. Reifenberg, K.-W. Chang, M. A. Panzer, S. Kim, J. A. Rowlette, M. Asheghi, H.-S. P. Wong, and K. E. Goodson, IEEE Electron Device Lett. **31**(1), 56–58 (2010).
[14]J. Lee, Z. Li, J. P. Reifenberg, M. Asheghi, and K. E. Goodson, J. Appl. Phys. **109**, 084902 (2011).
[15]J. Lee, S. Kim, R. Jeyasingh, M. Asheghi, H.-S. P. Wong, and K. E. Goodson, IEEE Electron Device Lett. **32**(7), 952–954 (2011).
[16]H.-S. P. Wong, S. Raoux, S. Kim, J. Liang, J. P. Reifenberg, B. Rajendran, M. Asheghi, and K. E. Goodson, Proc. IEEE **98**(12), 2201 (2010).
[17]J. A. Rowlette, R. D. Kekatpure, M. A. Panzer, M. L. Brongersma, and K. E. Goodson Phys. Rev. B **80**(4), 045314 (2009).
[18]R. B. Wilson and D. G. Cahill, Phys. Rev. Lett. **108**, 255901 (2012).
[19]W. M. Loh, S. E. Swirhun, E. Crabbe, K. Saraswat, and R. M. Swanson, IEEE Electron Device Lett. **6**, 441–443 (1985).
[20]M. Finetti, A. Scorzoni, and G. Soncini, IEEE Electron Devices Lett. **5**(12), 524–526 (1984).
[21]M. Ono, A. Nishiyama, and A. Toriumi, Solid-State Electron. **46**, 1325–1331 (2002).
[22]H. K. Peng, K. Cil, A. Gokirmak, G. Bakan, Y. Zhu, C. S. Lai, C. H. Lam, and H. Silva, "Thickness dependence of the amorphous-cubic and cubic-hexagonal phase transition temperatures of GeSbTe thin films on silicon nitride," Thin Solid Films **520**, 30123 (2011).
[23]J. Lee, T. Kodama, Y. Won, M. Asheghi, and K. E. Goodson, J. Appl. Phys. **112**, 014902 (2012).
[24]R. E. Simpson, M. Krbal, P. Fons, A. V. Kolobov, J. Tominaga, T. Uruga, and H. Tanida, Nano Lett. **10**, 414–419 (2010).
[25]S. Raoux, J. L. Jordan-Sweet, and A. Kellock, J. Appl. Phys. **103**, 114310 (2008).
[26]D. G. Cahill, S. K. Watson, and R. O. Pohl, Phys. Rev. B **46**, 6131 (1992).
[27]P. Kivinen, A. Savin, M. Zgirski, P. Törmä, J. Pekola, M. Prunnial, and J. Ahopelto, J. Appl. Phys. **94**, 3201 (2003).
[28]G. S. Kumar, G. Prasad, and R. O. Pohl, J. Mater. Sci. **28**, 4261–4272 (1993).
[29]S. Yoneoka, J. Lee, M. Liger, G. Yama, T. Kodama, J. Provine, R. T. Howe, K. E. Goodson, and T. W. Kenny, Nano Lett. **12**, 683–686 (2012).
[30]G. D. Mahan and M. Bartkowiak, Appl. Phys. Lett. **74**(7), 953–954 (1999).
[31]D. Roy, M. A. A. in't Zandt, and Rob A. M. Wolters, IEEE Electron Device Lett. **31**(11), 1293–1295 (2010).
[32]A. Y. C. Yu, Solid-State Electron. **13**, 239–247 (1970).
[33]P. N. Vinod, J. Alloys Compd. **470**, 393–396 (2009).
[34]A. Majumdar and P. Reddy, Appl. Phys. Lett. **84**(23), 4768–4770 (2004).
[35]D. Chen, J. Chen, Y. Zhao, B. Yu, C. Wang, and D. Shi, Acta Metall. Sin. (Engl. Lett.) **22**(2), 146–152 (2009).
[36]Y. Won, J. Lee, M. Asheghi, T. W. Kenny, and K. E. Goodson, Appl. Phys. Lett. **100**, 161905 (2012).
[37]E. Schwartz and R. Pohl, "Thermal boundary resistance," Rev. Mod. Phys. **61**(3), 605–668 (1989).
[38]L. De Bellis, P. E. Phelan, and R. S. Prasher, J. Thermophys. Heat Transfer **14**(2), 144–150 (2000).
[39]See supplementary material at http://dx.doi.org/10.1063/1.4807141 for electrical contact resistance, TDTR, and XRD measurement details.